AJG

Article

Man-made Structure Extraction Based on Scattering Decomposition Using PolSAR Data

Yasumin Siriprathan[1], Junichi. Susaki*[2], Yoshie Ishii[3] and Tetsuharu Oba[4]

[1]Graduate School of Engineering, Kyoto University, Kyotodaigaku Katsura, Nishikyoku, Kyoto 615-8540, Japan. Email: <siriprathan.yasumin.64u@st.kyoto-u.ac.jp>

[2]Professor, Graduate School of Engineering, Kyoto University, Kyotodaigaku Katsura, Nishikyoku, Kyoto 615-8540, Japan. Email:<susaki.junichi.3r@kyoto-u.ac.jp>

[3]Assistant Professor, Graduate School of Engineering, Kyoto University, Kyotodaigaku Katsura, Nishikyoku, Kyoto 615-8540, Japan. Email:<ishii.yoshie.4k@kyoto-u.ac.jp>

[4]Professor, Graduate School of Management & Graduate School of Engineering, Kyoto University, Kyotodaigakukatsura, Nishikyo-ku, Kyoto, 615-8540, Japan. Email: <oba.tetsuharu.5n@kyoto-u.ac.jp>

*Corresponding author: J. susaki, Email: <susaki.junichi.3r@kyoto-u.ac.jp>

Received: November 21, 2024; Accepted: April 3, 2025; Published: April 15, 2025

ABSTRACT

Man-made structure extraction is essential for urban planning, environmental monitoring, and disaster management. Optical sensors often face limitations due to weather and lighting conditions; in comparison, synthetic aperture radar (SAR) provides consistent imaging in all environments. This study leveraged Polarimetric SAR (PolSAR) data and advanced scattering decomposition techniques to enhance the extraction of man-made structures. The methodology involved the collection of microwave scattering data from concrete blocks at various angles within an anechoic chamber, which was then used to train machine learning models. These models were subsequently applied to real-world satellite data from the Advanced Land Observing Satellite-2/Phased Array type L-band Synthetic Aperture Radar-2 (ALOS-2/PALSAR-2) to ensure practical applicability of the approach. Scattering decomposition significantly improved the detection accuracy compared with using the original scattering data alone, offering a clearer identification of man-made structures. Incorporating the polarimetric orientation angle further enhances the classification accuracy, making it a valuable addition to the method. Our approach offers significant insights into the planning and management of sustainable man-made structures and resources.

Keywords: Man-made structure extraction, Polarimetric SAR, Scattering decomposition, Machine learning, Polarimetric orientation angle

1. INTRODUCTION

The rapid growth of cities worldwide, particularly in densely populated areas, such as Asia, has led to serious challenges including insufficient infrastructure, environmental problems, and increased risks from natural

disasters. As cities expand, accurate and up-to-date maps of urban areas have become essential for sustainable planning and disaster management (Kajimoto & Susaki, 2013a). However, conventional mapping methods often relying on Geographic Information Systems (GIS) and optical imagery can be slow to update and are limited by weather conditions, making them less effective in tracking rapid urban growth (Li et al., 2016).

In this context, synthetic aperture radar (SAR) has become a valuable tool for mapping man-made structures. It provides high-resolution images under various light and weather conditions (Yamaguchi et al., 2020). Polarimetric SAR (PolSAR) adds to this capability with the use of multiple polarization channels that provide detailed information on the scattering properties of surfaces, which helps distinguish man-made structures from natural features (Niu & Ban, 2012). Despite these advantages, interpreting PolSAR data is challenging because of complex backscattering in dense man-made structural areas, where interactions between different surfaces can complicate the analysis (Freeman & Durden, 1998; Shabou et al., 2012).

Many studies have shown that PolSAR data are useful for the extraction and classification of urban areas. For example, Freeman and Durden (1998) developed a three-component scattering model to explain urban scattering patterns, whereas Yamaguchi et al. (2006) proposed a four-component decomposition method to better classify scattering types. Kimura (2008) and Lee et al. (2000) also examined how polarimetric orientation angle (POA) shifts can reveal information on building orientations, helping to improve urban mapping accuracy. More recently, Kajimoto and Susaki (2013b) applied POA correction methods to estimate urban density, highlighting new ways to enhance urban mapping using PolSAR data.

Building on this prior work, this study introduces a new method for extracting man-made structures by combining PolSAR data using advanced scattering decomposition techniques. Our approach uses Yamaguchi's four-component decomposition model along with POA estimation to improve the accuracy of artificial feature extraction (Yamaguchi et al., 2006). In addition, we incorporated a random forest (RF) classifier trained on experimental data from concrete blocks, which we applied to the Advanced Land Observing Satellite-2/Phased Array-type L-band Synthetic Aperture Radar-2 (ALOS-2/PALSAR-2) satellite data. By integrating the POA and machine learning, our method aims to provide a more precise solution for mapping man-made structures (Ferretti et al., 2011).

The rest of this paper is organized as follows. In Section 2, we explain the indices used in our methodology, including the scattering matrix (S-matrix), coherency matrix (T-matrix), four-component decomposition, POA estimation, K-means clustering, and RF classification. Section 3 describes the experimental and satellite datasets used in this study. Section 4 details the methods applied. In Section 5, we present and discuss the classification results. Finally, Section 6 presents conclusions and recommendations for future research.

2. INDICES USED

In this section, we discuss the various indices used in this study for man-made structure extraction and classification using Polarimetric

SAR (PolSAR) data. These indices include the scattering matrix (S-matrix), coherency matrix (T-matrix), four-component decomposition, POA estimation, K-means clustering, and the RF classification algorithm. Each index plays a crucial role in enhancing the accuracy of man-made structure extraction and classification.

2.1 Scattering Matrix (S-matrix)

The scattering matrix (S-matrix) is fundamental for describing the scattering behavior of a target in PolSAR. It captures the complex amplitudes of the scattered field across different polarizations. The scattering matrix is fundamental for describing target scattering behavior in PolSAR and is commonly expressed as follows (Lee & Pottier, 2009):

$$S = \begin{pmatrix} S_{HH} & S_{HV} \\ S_{VH} & S_{VV} \end{pmatrix} \quad (1)$$

Here, S_{HH} and S_{VV} represent the co-polarized backscatter for horizontal and vertical polarizations, respectively, whereas S_{HV} and S_{VH} represent the cross-polarized backscatter. For simplicity, S_{HV} and S_{VH} are assumed to be equivalent. This scattering matrix serves as the foundation for further decomposition and classification techniques in PolSAR analyses.

2.2 Coherency Matrix (T-matrix)

The coherency matrix T derived from the scattering matrix represents the second-order statistics of the scattering mechanism, capturing power and correlation properties. The coherency matrix, introduced in the context of PolSAR data processing, is defined as follows (Cloude & Pottier, 1996):

$$T = \begin{pmatrix} T_{11} & T_{12} & T_{13} \\ T_{21} & T_{22} & T_{23} \\ T_{31} & T_{32} & T_{33} \end{pmatrix} = \begin{pmatrix} \frac{\langle |S_{HH}+S_{VV}|^2 \rangle}{2} & \frac{\langle (S_{HH}+S_{VV})(S_{HH}-S_{VV})^* \rangle}{2} & \langle (S_{HH}+S_{VV}) S^*_{HV} \rangle \\ \frac{\langle (S_{HH}+S_{VV})^*(S_{HH}-S_{VV}) \rangle}{2} & \frac{\langle |S_{HH}-S_{VV}|^2 \rangle}{2} & \langle (S_{HH}-S_{VV}) S^*_{HV} \rangle \\ \langle (S_{HH}+S_{VV})^* S_{HV} \rangle & \langle (S_{HH}-S_{VV})^* S_{HV} \rangle & \langle 2|S_{HV}|^2 \rangle \end{pmatrix} \quad (2)$$

This matrix provides a comprehensive description of the scattering process by accounting for the coherency and phase differences between polarizations. Different elements of the matrix are related to specific scattering mechanisms: T_{11} represents surface scattering, T_{22} represents double-bounce scattering, and T_{33} represents volume scattering (Yamaguchi et al., 2020). Other elements, such as T_{12}, T_{13}, and T_{23}, represent additional scattering processes.

2.3 Four-component Decomposition

The four-component decomposition method divides the observed backscattering into four distinct components derived from the coherency matrix. When applied to a full PolSAR dataset, this method provides surface scattering power (Ps), double-bounce scattering power (Pd), volume scattering power (Pv), and helix scattering power (Ph) (Yamaguchi et al., 2006).

To address the dependence on the POA, Yamaguchi et al. (2006) introduced a rotation of the coherency matrix based on the POA, helping to reduce the azimuthal effects on these components. Here, θ represents the POA, which indicates the orientation angle of the target structure relative to the radar's line of sight. This rotation can be expressed as:

$$T(\theta) = \begin{pmatrix} T_{11}(\theta) & T_{12}(\theta) & T_{13}(\theta) \\ T_{21}(\theta) & T_{22}(\theta) & T_{23}(\theta) \\ T_{31}(\theta) & T_{32}(\theta) & T_{33}(\theta) \end{pmatrix} = \left[R_p(\theta)\right]^{\dagger} \cdot T \cdot R_p(\theta) \quad (3)$$

$R_p(\theta)$ is the rotation matrix defined as:

$$R_p(\theta) = \begin{pmatrix} 1 & 0 & 0 \\ 0 & cos2\theta & sin2\theta \\ 0 & -sin2\theta & cos2\theta \end{pmatrix} \quad (4)$$

This decomposition and rotation operation helps isolate the contributions from each scattering mechanism by aligning the coherency matrix with the POA.

2.4 Polarimetric Orientation Angle (POA) Estimation

The POA is critical for accurately representing the orientation angle of the target structure relative to the line-of-sight of the radar. The POA can be estimated using the following equation:

$$\theta = \frac{1}{4}\tan^{-1}\left(\frac{2Re(T_{23})}{(T_{22})-(T_{33})}\right), \left(-\frac{\pi}{4} \le \theta \le \frac{\pi}{4}\right) \quad (5)$$

Here, Re denotes the real part of the complex number, and T_{22}, T_{23}, and T_{33} are the elements of the coherency matrix. Incorporating POA into classification models enhances the accuracy of feature extraction for man-made structures by correcting the angular effects caused by the orientation of the structure (Kajimoto & Susaki, 2013).

The POA can be conceptualized as the angle of rotation around the radar's line of sight. The transformation of a scattering matrix rotated by an orientation angle ξ is represented as:

$$S(\xi) = \begin{pmatrix} cos\xi & sin\xi \\ -sin\xi & cos\xi \end{pmatrix} \begin{pmatrix} S_{HH} & S_{HV} \\ S_{VH} & S_{VV} \end{pmatrix} \begin{pmatrix} cos\xi & -sin\xi \\ sin\xi & cos\xi \end{pmatrix}$$

In media with reflection symmetry, such as flat horizontal surfaces, the POA is typically zero (Lee et al., 2000). However, in complex environments with steep terrain or inclined man-made structures, the POA often deviates from zero because of non-horizontal surfaces, buildings, and bridges that are not aligned with the radar's flight path (Lee et al., 2002). Accurately accounting for these variations is crucial for effective terrain modeling and feature classification, leading to more reliable results (Lee et al., 2002; Ainsworth et al., 2008).

2.5 K-means Clustering

The K-means clustering algorithm can be defined mathematically as follows:

$$J = \sum_{i=1}^{k}\sum_{j=1}^{n}\left\|x_j - \mu_i\right\|^2 \quad (7)$$

Here:

n: total number of data points in the dataset.
J: objective function to minimize.
k: number of clusters.
x_j: data point.
μ_i: centroid of cluster i.

K-means clustering was selected for its simplicity, efficiency, and ability to dynamically classify man-made and non-man-made structural areas in experimental datasets without the need for manual labelling.

2.6 Random Forest Classification

The RF algorithm was used as a machine learning classifier to categorize man-made structural features based on the indices discussed. It is an ensemble-learning method that constructs multiple decision trees during training and outputs the class, which is the mode of the classes (for classification) or the mean prediction (for

regression) of individual trees. This algorithm is particularly effective for handling high-dimensional data and capturing complex interactions between features (Breiman, 2001).

3. DATA

3.1 Experimental PolSAR Data

The experimental dataset comprises backscattering measurements at various orientation angles and distances recorded at the X-band frequency. These data were collected from 20–21 September 2011 using a fully polarimetric SAR system in an anechoic chamber at Niigata University. Polarizations HH, HV, VH, and VV are crucial for extracting and classifying man-made structures. These experimental data enhance the model accuracy by providing precise scattering characteristics specific to man-made areas. Measurements were conducted on concrete blocks of sizes scaled according to the law of similarity to ensure a realistic representation of real-world conditions.

3.2 Advanced Land Observing Satellite-2/Phased Array type L-band Synthetic Aperture Radar-2 (ALOS-2/PALSAR-2)

In this study, we used the Advanced Land Observing Satellite-2/Phased Array-type L-band Synthetic Aperture Radar-2 (ALOS-2/PALSAR-2) dataset, an advanced L-band (1.27 GHz) synthetic aperture radar system operated by the Japan Aerospace Exploration Agency (JAXA), to map large-scale man-made structures in Tokyo and Bangkok. Two specific datasets were employed: one acquired over Tokyo on May 7, 2024, during an ascending orbit, and the other acquired over Bangkok on April 27, 2024. Each dataset offers a high spatial resolution of 6 m and includes crucial polarimetric data comprising amplitude and phase information, which are essential for distinguishing between man-made structures and natural surfaces. This distinction is made possible by the capability of the dataset to reveal surface characteristics, such as roughness and dielectric properties, which differ significantly between artificial and natural materials.

The versatility of ALOS-2/PALSAR-2 in polarimetric modes (HH, HV, and VV) enhances its sensitivity to various surface types, making it particularly suitable for the detection and classification of man-made structures. These polarimetric modes provide comprehensive insights into surface reflections, as shown in Fig. 2. The PolSAR image from Tokyo (Figure 2a) displays a color composite (Red: HH, Green: HV, Blue: VV), providing a clear visual distinction between the features related to man-made structures. Similarly, the Bangkok PolSAR image (Figure 2b) uses the same color composite to highlight the surface variations in areas containing artificial structures. Table 1 outlines the specific details of the PolSAR images used in this experiment and supports the methodology and results by clarifying the study area, acquisition dates, and off-nadir angles. These high-resolution polarimetric ALOS-2/PALSAR-2 datasets effectively facilitate the analysis and mapping of man-made structures in complex urban environments.

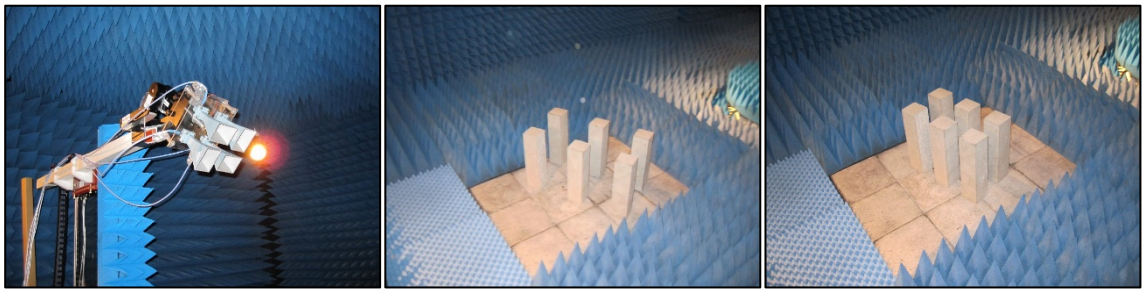

Figure 1: Setup of the microwave scattering measurement experiment in an anechoic chamber at Niigata University.

Table 1: Details of PolSAR images used for the experiment.

City	Observation date [yyyy/mm/dd]	Off-nadir angle
Tokyo	2024-05-07	25.0°
Bangkok	2024-04-27	32.7°

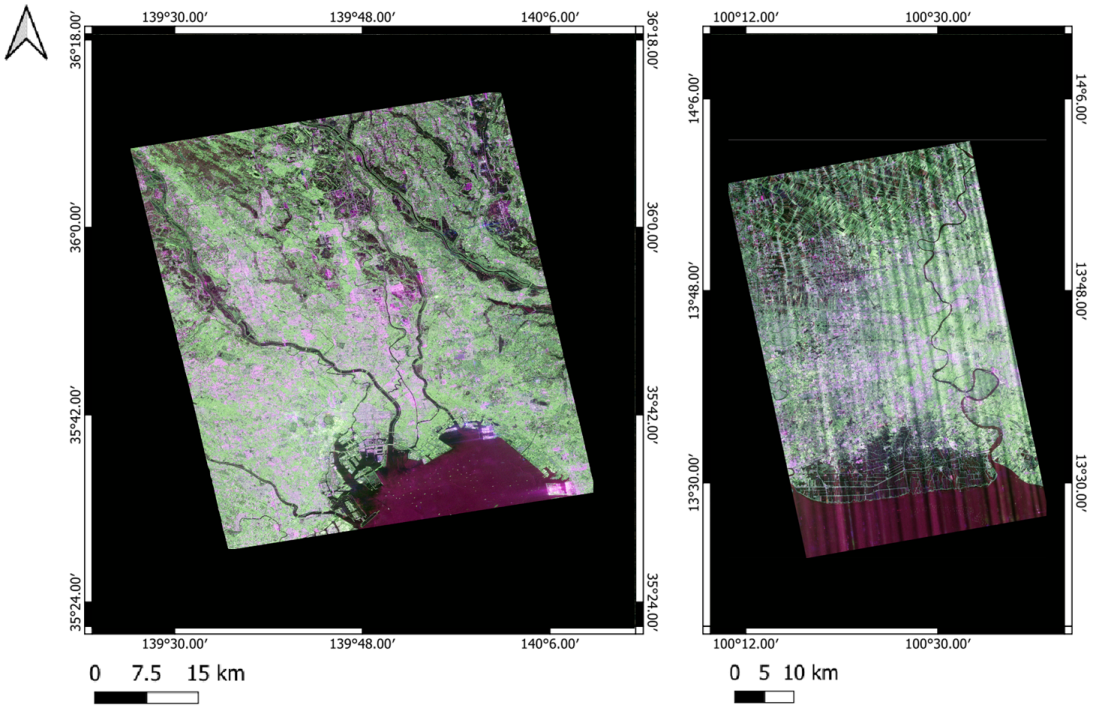

(a) (b)

Figure 2: PolSAR images acquired with the ALOS2/PALSAR2: (a) PolSAR image in Tokyo (Red: HH, Green HV, Blue VV) and (b) PolSAR image in Bangkok (Red: HH, Green HV, Blue VV)

4. METHOD

4.1 Training Dataset Preparation

The training dataset for this study was derived from experimental PolSAR data measurements conducted at Niigata University, which included microwave scattering data collected from concrete blocks at various azimuth angles. The dataset includes approximately over 600,000 pixels for both the non-man-made and man-made structural classes, ensuring a balanced representation and minimizing bias. Data

normalization techniques were applied to address imbalanced features. Initially, K-means clustering was employed to identify the natural groupings within the data, which were then used to label the man-made and non-man-made structural classes. These labeled data points served as the foundation for subsequent model training. Figure 3 illustrates an example of the clustering results from the X-band scattering experiment used to classify man-made structures. The values in brackets indicate the minimum and maximum backscattering intensity (in dB) observed in each polarization channel.

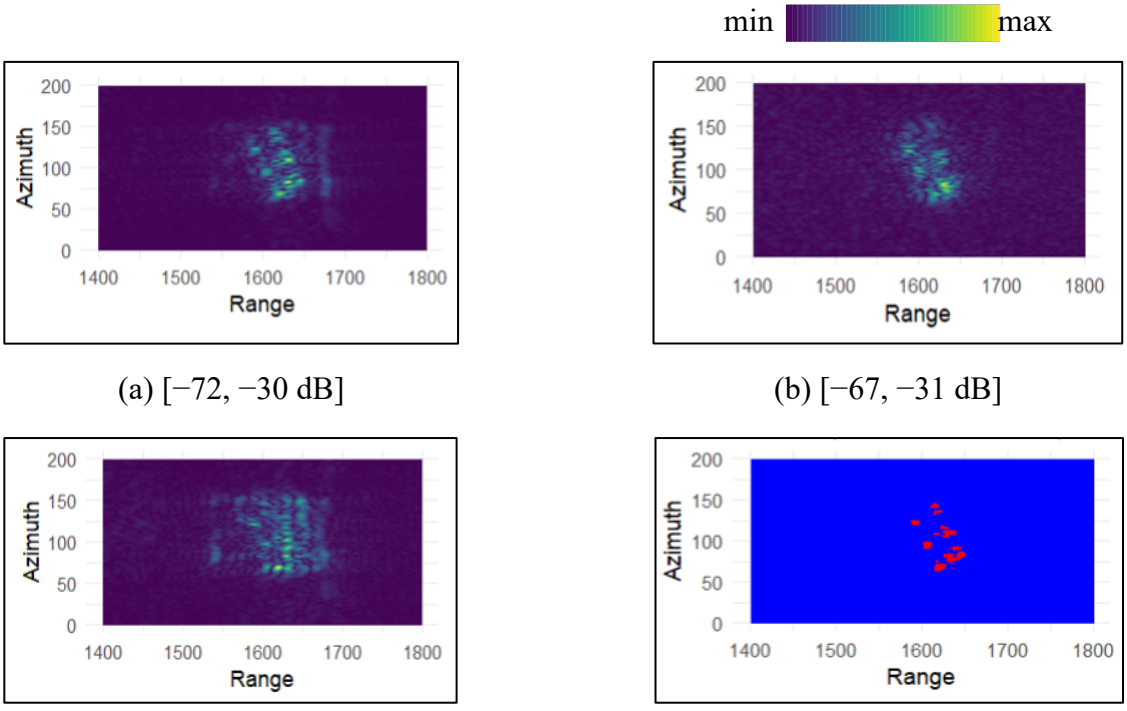

(a) [−72, −30 dB] (b) [−67, −31 dB]

(c) [−71, −29 dB] (d)

Figure 3: X-band scattering experiment clustering results for man-made structure classification (a) HH, (b) HV, (c) VV, and (d) classification (red: man-made, blue: non-man-made).

4.2 Classification Using Original Scatterings

The initial step in our methodology involves the direct classification of man-made structural areas using the original PolSAR data scatterings: HV, VH, VV, and HH. These scatterings, representing the horizontal and vertical polarization states, contain vital information regarding the backscatter from various man-made structural features. The intensity of each pixel in these scatterings reflects the strength of the radar signal, which interacts with objects in the scene. An RF classifier was trained using these original data scatterings to establish a baseline for man-made structure feature classification. This approach allowed us to evaluate the discriminative power of the original scatterings to distinguish between different man-made and non-man-made structural classes without additional feature extraction.

4.3 Classification Using Scattering Decomposition

In the next phase, we applied the four-component scattering decomposition technique based on Yamaguchi's decomposition model to

PolSAR data. This technique decomposes the SAR signal into four scattering mechanisms: surface scattering (*Ps*), double-bounce scattering (*Pd*), volume scattering (*Pv*), and helix scattering (*Ph*). By using these decomposed components as features in our RF classifier, we aimed to improve the classification accuracy by capturing more detailed physical characteristics of man-made structural areas, which are often mixed and complex in nature.

4.4 Classification Using Scattering Decomposition + POA

The third stage of the methodology introduces an advanced classification technique that integrates scattering decomposition with the POA as an additional feature. Scattering decomposition techniques, such as Yamaguchi's four-component model, decompose PolSAR data into distinct scattering mechanisms: *Ps*, *Pd*, *Pv*, and *Ph*. By incorporating the POA into the decomposition process, we aimed to correct for orientation-induced distortions, which are prevalent in man-made structural areas due to the varied alignment of the structure. The classifier, trained with *Ps*, *Pd*, *Pv*, *Ph*, and POA, is expected to yield more accurate man-made structure feature extraction by accounting for both the scattering characteristics and orientation of man-made structural features. Figure 4 presents a flowchart of the proposed study, outlining the methodology followed at each stage.

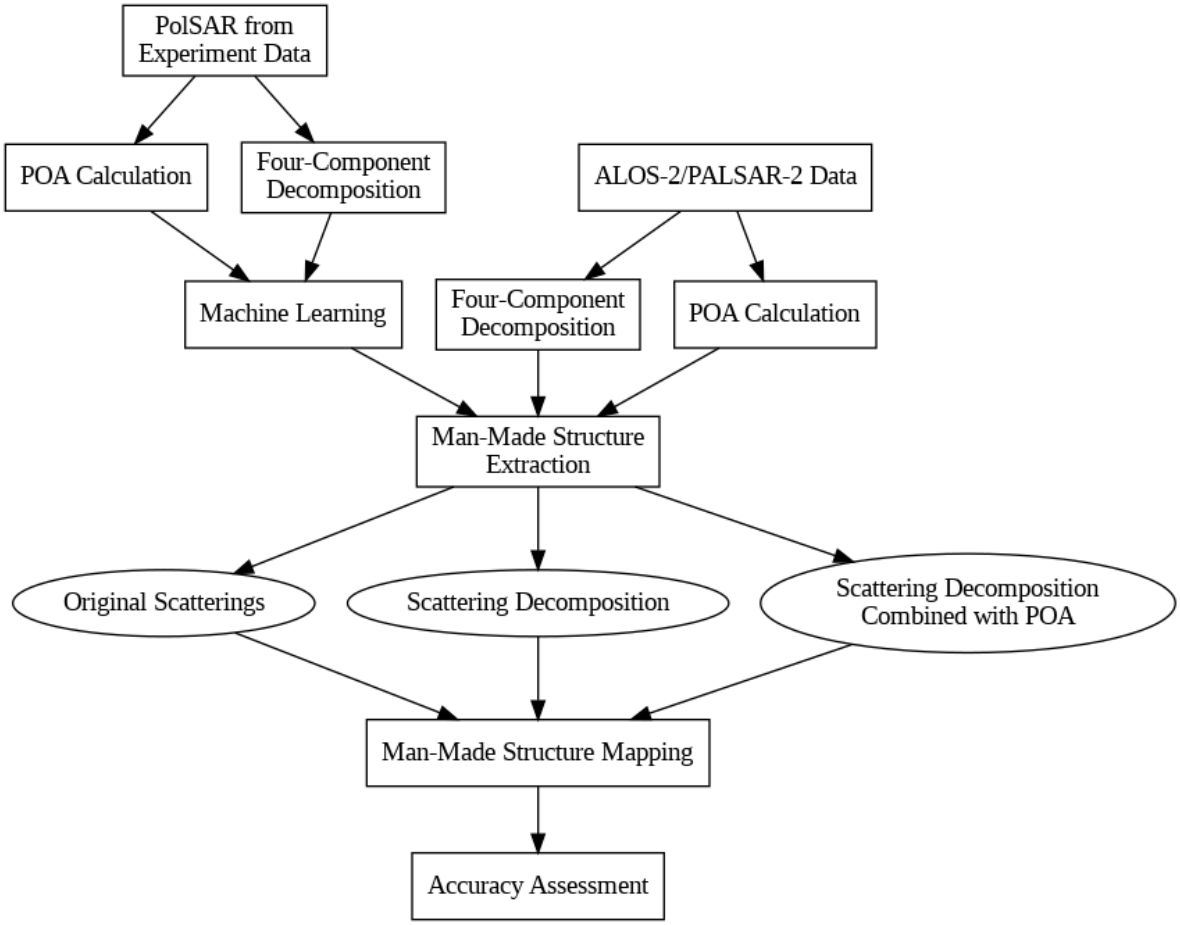

Figure 4: Flowchart of the proposed study methodology.

4.5 Hyperparameter Tuning

The RF model used in the classification stage underwent hyperparameter tuning using a random-search approach. The adjusted primary hyperparameters were mtry (the number of variables randomly sampled as candidates at each split) and ntree (the number of trees in the forest). The tuning range for mtry was set between 2 and 10, while for ntree, it was between 50 and 200. While increasing ntree can improve performance, it also increases computation time. In this study, mtry was set to 2, and ntree to 100, based on preliminary experiments to optimize model performance.

4.6 Validation Method

The classification results were validated by comparing the classification results from the Advanced Land Observing Satellite-2/Phased Array type L-band Synthetic Aperture Radar-2 (ALOS-2/PALSAR-2), derived from man-made structural areas, with the built area class from the Sentinel-2 land cover dataset. Sentinel-2's annually updated land-cover dataset was produced using deep learning AI models and a large training dataset (Karra et al., 2021). While Sentinel-2 includes several land-cover classes, we focused solely on the built area class to validate man-made structures, specifically targeting dense structures such as buildings and elevated constructions.

Because the training dataset was based on the scattering characteristics of concrete blocks, which are highly sensitive to dense man-made structures, such as buildings, certain urban features, such as flat paved surfaces (e.g., roads and runways) or low-density urban areas, were initially underrepresented. To address this issue and refine our focus on higher-density structures, we manually excluded ground-level features such as roads, parking lots, and runways from the Sentinel-2 dataset.

To reconcile the resolution differences between ALOS-2/PALSAR-2 (6 m) and Sentinel-2 (10 m), we applied nearest-neighbor resampling to ensure pixel alignment for accurate comparison.

As a cautionary note, it is important to consider potential errors in the Sentinel-2 land-cover dataset, as land-cover maps may include classification inaccuracies. According to Karra et al. (2021), the Sentinel-2 land cover dataset achieved an overall accuracy of 85% across all ten classes of holdout validation tiles. In addition, a more detailed accuracy assessment per class is available across four regions (California, Costa Rica, Belgium, and Laos), with an error matrix of the estimated area proportions for each region, along with the user and producer accuracies. The study also computed the class area with 95% confidence error bounds based on the error matrix in each region. This serves as a reference for the expected accuracy of the Sentinel-2 dataset, which must be considered when interpreting our validation results.

For the accuracy assessment in our study, we calculated the Overall Accuracy (OA), Producer's Accuracy (PA), and User's Accuracy (UA) for both man-made and non-man-made structures, with a focus on dense man-made features to enhance the classification accuracy compared with general man-made structure classifications.

5. RESULTS AND DISCUSSION

This study focuses on the extraction and

classification of man-made structures using Polarimetric Synthetic Aperture Radar (PolSAR) data to evaluate the performance of various classification techniques. The classification results were validated using an updated ground truth dataset from Sentinel-2, which provides high-resolution, 10-m land cover data for 2024 (Karra et al., 2021). In this updated dataset, we manually excluded ground-level features, such as roads, runways, and parking lots, resulting in a significant improvement in the overall accuracy of the classification of dense, elevated structures compared with the previous "urban" category. Nevertheless, challenges persist, particularly in misclassifying areas with scattering from oriented targets, resulting in the occasional confusion between volume and double-bounce scattering.

5.1 Comparative Analysis of Classification Approaches

Several studies have explored the effectiveness of polarimetric decomposition methods for land cover classification. Wang et al. (2022) examined dryland crop classification using GF3 full-polarimetric SAR data, finding that a multi-component decomposition method achieved an overall accuracy of 88.37%. This underscores the advantage of leveraging multiple scattering mechanisms to improve classification. Similarly, Srivally et al. (2024) compared commonly used decomposition techniques, reporting overall accuracies of 79.6% and 81.9% for the Freeman–Durden and Yamaguchi methods, respectively. These results indicate that different decomposition techniques capture distinct scattering characteristics, affecting classification performance. However, most existing studies focus on general land cover classification rather than specifically extracting man-made structures.

Our research aims to improve the accuracy of elevated man-made structure classification using PolSAR data. Many classification methods misinterpret open spaces such as paved surfaces, parking lots, and golf courses as built-up areas due to similar scattering properties. In contrast, our approach integrates scattering decomposition with Polarimetric Orientation Angle (POA) estimation to enhance the differentiation between dense, elevated urban structures and open, flat surfaces.

Applying this method to man-made and non-man-made land cover classification in Tokyo and Bangkok (2024), we achieved overall accuracies of 90.42% and 92.35%, respectively. These results demonstrate a significant improvement over conventional decomposition methods. The inclusion of POA helps account for structural orientation effects, which are often overlooked in traditional classification. This is particularly important for distinguishing high-rise buildings and dense urban infrastructure from paved areas that exhibit similar scattering behavior but lack vertical structures.

To further validate our approach, we compared our results with high-resolution Sentinel-2 reference data. Costa et al. (2021) showed that integrating ALOS-2/PALSAR-2 and Sentinel-2A data yielded an overall accuracy of 85.56%, while Sentinel-2A alone provided comparable results. Our findings align with this but offer a significant advantage in man-made structure classification. By integrating scattering decomposition with POA, our method reduces confusion between built-up areas and similar land cover types, making it highly effective for urban mapping, infrastructure monitoring, and disaster assessment.

5.2 Close-Up Analysis of Classification Accuracy Using Sentinel-2 Data

To further validate the classification performance, we compare ALOS-2 PolSAR classification results with Sentinel-2 optical imagery, which serves as a high-resolution reference dataset. Figures 5 and 6 show a close-up view of selected manmade structure areas in Tokyo and Bangkok, respectively, illustrating classification results obtained from our method alongside Sentinel-2 reference data.

Figure 5 provides a detailed comparison of manmade structure classification in Tokyo. The proposed method effectively captures major man-made structures and their spatial distribution, aligning well with the Sentinel-2 reference data, particularly in high-density urban zones. Notably, our classification approach demonstrates a clear distinction between vegetation and built-up areas, reducing misclassification of green spaces as manmade infrastructure. Additionally, the method accurately identifies open paved surfaces, such as large parking lots and sports fields, as non-manmade structures. This contrasts with the Sentinel-2 reference dataset, which classifies certain open areas, including sports complexes and racecourses, as built-up regions.

Figure 6 presents a close-up comparison of manmade structure classification in Bangkok. The proposed method exhibits strong performance in distinguishing water bodies, and agricultures from manmade structure region. This enhanced differentiation is particularly beneficial in regions with complex hydrological networks, such as canal-dense areas.

These comparisons highlight the advantages of PolSAR-based classification in capturing principle manmade features with improved precision. However, some discrepancies remain in mixed land cover regions where scattering similarities may lead to minor classification errors. While our method enhances manmade structure distinction, incorporating additional contextual information from multi-temporal SAR or optical sources could further refine classification accuracy. Future research could explore deep learning-based fusion techniques to enhance manmade structure extraction and reduce classification ambiguities.

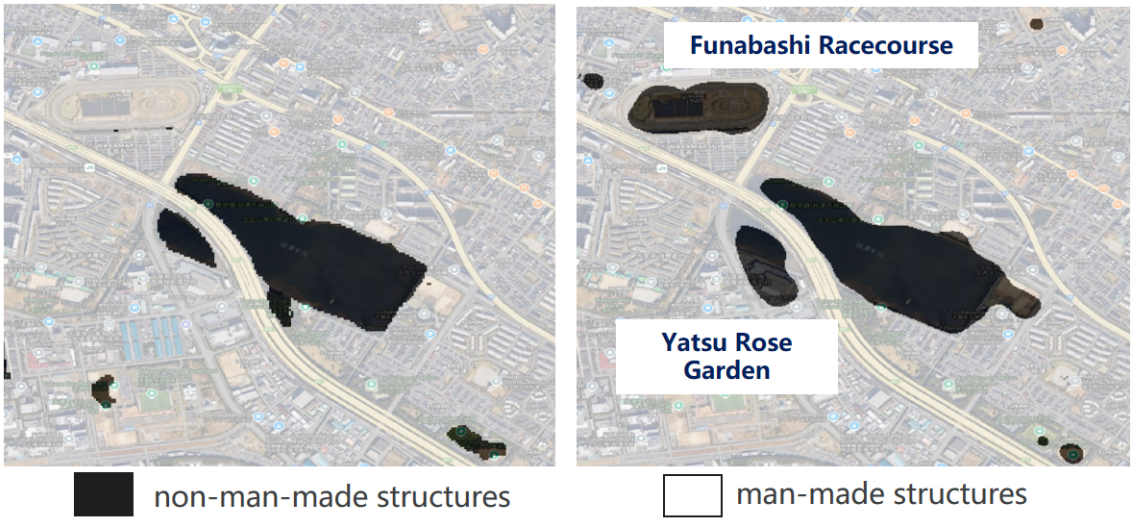

Figure 5: Close-up comparison of manmade structure classification in Tokyo (Left: Sentinel-2 reference, Right: ALOS-2 classification).

Figure 6: Close-up comparison of manmade structure classification in Bangkok (Left: Sentinel-2 reference, Right: ALOS-2 classification.

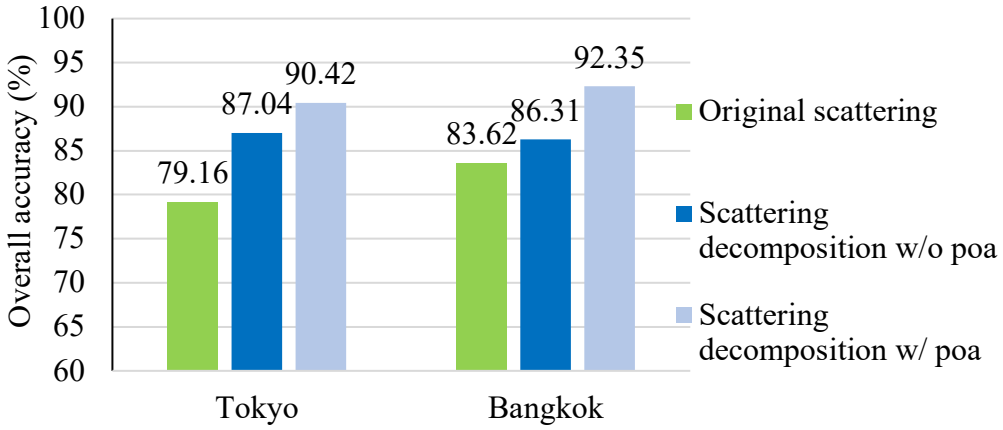

Figure 7: Overall accuracy (OA) for man-made structure classification in Tokyo and Bangkok using the three classification approaches

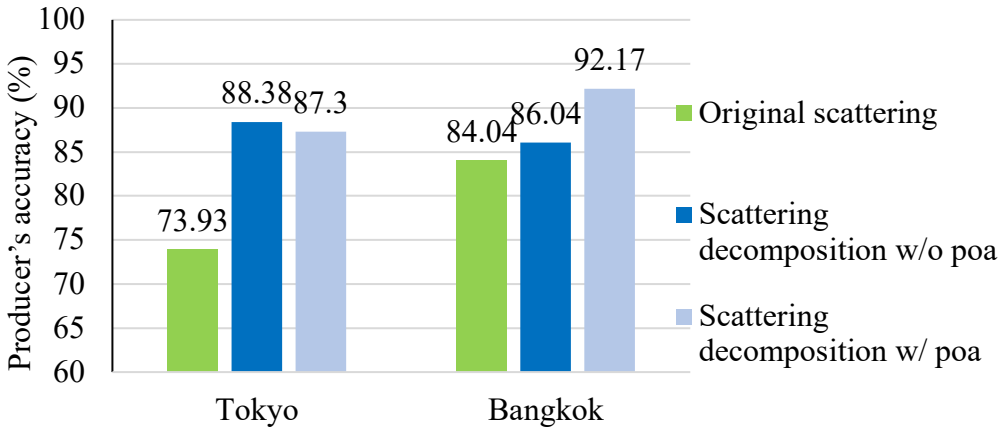

Figure 8: Producer's accuracy (PA) for each classification method in Tokyo and Bangkok

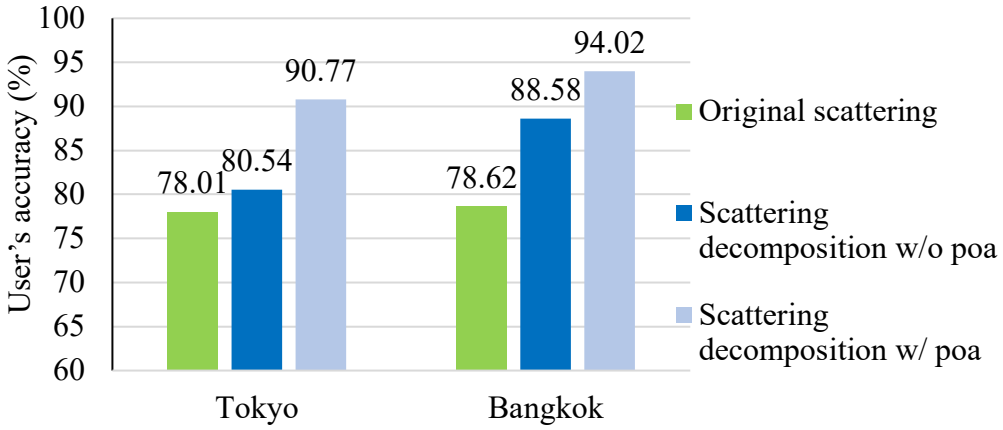

Figure 9: User's accuracy (UA) for each classification method in Tokyo and Bangkok.

5.3 Classification Approaches

The classification of the man-made structural areas was performed using three different approaches:

a) Original scatterings: This method uses the original PolSAR data without decomposition.
b) Scattering decomposition: This approach leverages scattering decomposition methods to improve classification.
c) Scattering decomposition combined with POA: This method integrates the POA with scattering decomposition for further accuracy improvements.

These methods were evaluated in two urban environments, Tokyo and Bangkok, using the PA, UA, and OA metrics. These metrics offer a comprehensive view of the effectiveness of each method in identifying man-made structures.

5.4 Results Summary

In Tokyo, the original scattering approach achieved an OA of 79.16%. By employing scattering decomposition, the OA improved to 87.04%. The highest accuracy was attained with the integration of the POA, yielding an OA of 90.42%. This demonstrates the effectiveness of the POA in enhancing the classification performance.

Similarly, in Bangkok, the original scattering method yielded an OA of 83.65%, which increased to 86.31% with the scattering decomposition. The best results were observed with scattering decomposition combined with the POA, which achieved an OA of 92.35%. This significant improvement highlights the strength of the combined method for accurately classifying man-made structures in complex urban landscapes.

5.5 Detailed Method Analysis

In this section, we analyze the classification results obtained from different methodological approaches. The effectiveness of each approach is assessed based on Overall Accuracy (OA) and its ability to distinguish man-made structures from non-man-made environments.

5.5.1 Baseline Classification Using Original Scatterings

The baseline method utilizes the original PolSAR scattering intensities (HH, HV, VV) without any additional processing. The classification results achieved Overall Accuracies

(OAs) of 79.16% in Tokyo and 83.65% in Bangkok. However, misclassifications were observed, primarily when non-human-made features, such as dense vegetation and water bodies, were incorrectly classified as man-made structures. This indicates that relying solely on original scattering information may not be sufficient for precise urban extraction.

5.5.2 Improvement with Scattering Decomposition

To enhance classification performance, scattering decomposition was applied to separate different scattering mechanisms. This method significantly improved accuracy, achieving OAs of 87.04% for Tokyo and 86.31% for Bangkok. The decomposition allowed better differentiation between urban structures and natural features, reducing misclassification errors observed in the baseline method. The improvement highlights the importance of utilizing scattering mechanisms for more reliable classification.

5.5.3 Enhanced Accuracy with Scattering Decomposition and POA Integration

Further refinement was achieved by incorporating Polarimetric Orientation Angle (POA) into the scattering decomposition process. This approach provided the highest classification accuracy, with OAs reaching 90.42% for Tokyo and 92.35% for Bangkok. The inclusion of POA helped capture additional orientation-related information, leading to improved Producer's Accuracy (PA) and User's Accuracy (UA) for man-made structures. This demonstrates that integrating orientation parameters enhances the robustness of manmade structure extraction.

5.6 Observations from Difference Maps

Figures 11a and c show the differences between the original scattering and scattering decomposition approaches. The extensive blue areas indicate that scattering decomposition could detect more man-made structures than the original scattering. However, this approach tends to overestimate the presence of man-made features, as it may incorrectly classify some natural vegetation as man-made areas.

Figures 11b and d show the difference between the scattering decomposition and the decomposition with POA. The inclusion of POA helps refine the classification by reducing the overestimation of man-made structures, as indicated by the decrease in blue areas. Moreover, the red areas in these figures highlight newly identified man-made structures that were previously missed when using the scattering decomposition method alone.

POA adjustment allows for a better differentiation between vegetation and man-made features, particularly in areas where natural and man-made elements are closely intertwined. This improved accuracy is evidenced by the reduction in the blue (overestimated man-made) areas and the appearance of the red (newly detected man-made) areas in Figures 11b and d, respectively.

Overall, the incorporation of POA in the decomposition using the POA approach leads to a more balanced and precise classification, better distinguishing between complex man-made and natural features compared with the scattering decomposition method. This demonstrates the value of utilizing POA information to enhance the accuracy of man-made structural mapping using PolSAR data.

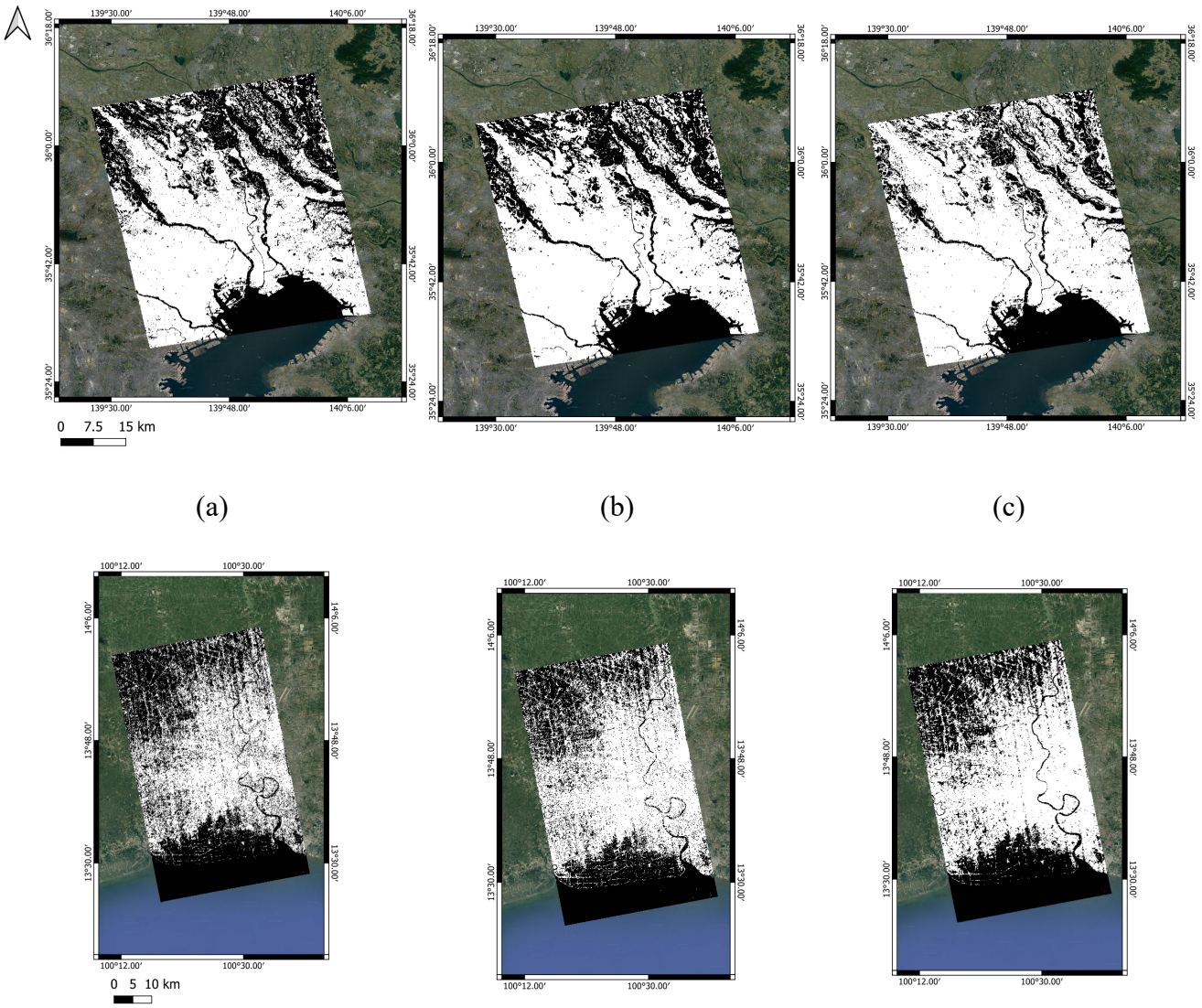

Figure 10: Results of the man-made structure classification results for Tokyo and Bangkok. The panels (a) and (d) show man-made structure classification using the original scatterings, (b) and (e) display man-made structure classification results using scattering decomposition, while (c) and (f) illustrate the classification results obtained using the proposed method, which combines scattering decomposition with the polarimetric orientation angle (POA).

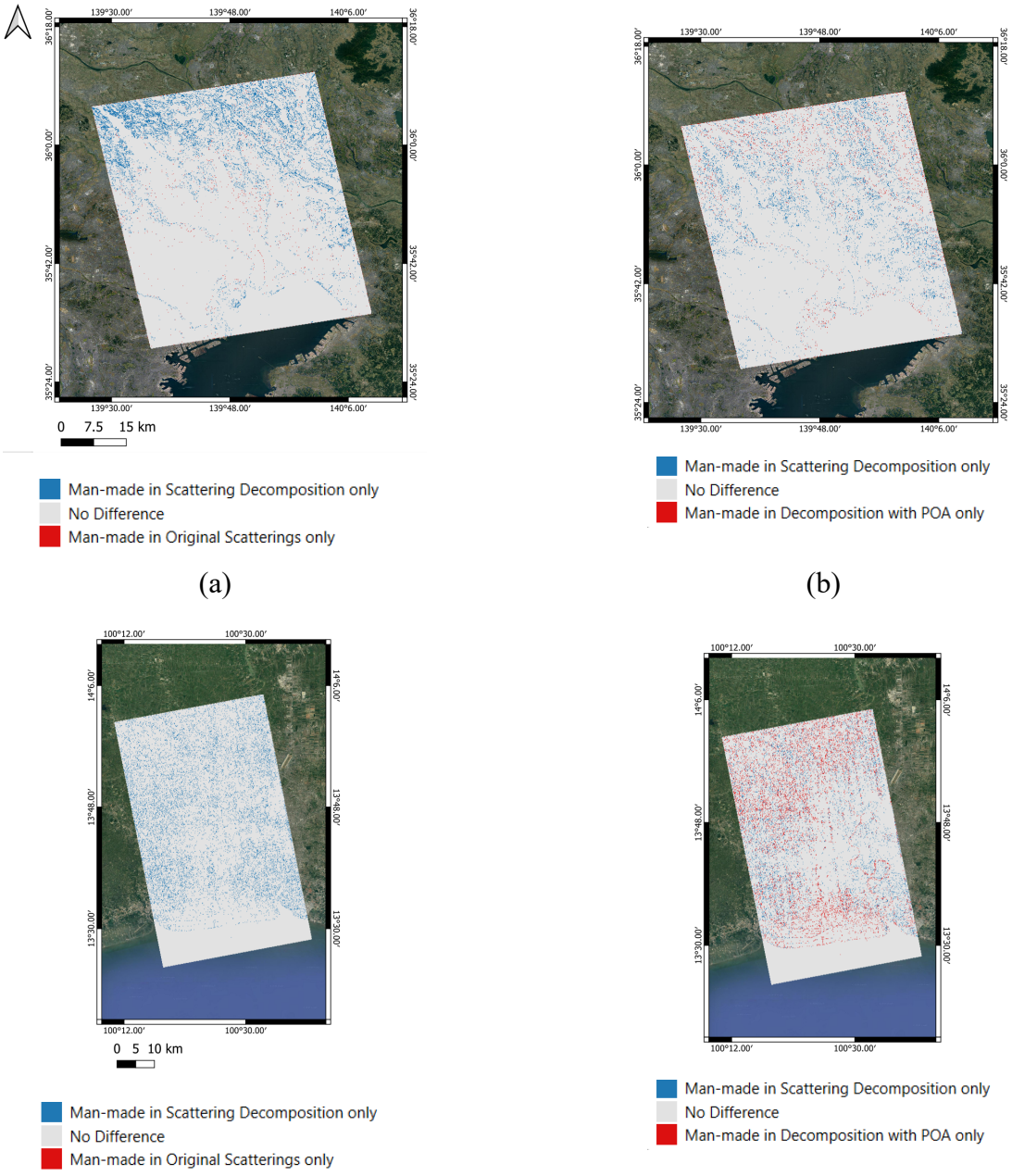

Figure 11: Difference maps for Tokyo and Bangkok areas: a) Difference map between original scatterings and scattering decomposition for Tokyo, b) Difference map between scattering decomposition and decomposition with POA for Tokyo, c) Difference map between original scatterings and scattering decomposition for Bangkok, d) Difference map between scattering decomposition and decomposition with POA for Bangkok.

5.7 Analysis of Misclassified Areas Using Sentinel-2 Land Cover Data

To better understand the limitations of our PolSAR classification method, we compared misclassified areas with Sentinel-2 land-cover classes. This analysis revealed that certain types of man-made structures, such as roads, parking lots, and industrial zones, are often misclassified as non-man-made. This misclassification occurred because these areas can exhibit

scattering characteristics similar to those of natural surfaces, leading to confusion during classification.

Specifically, flat paved surfaces typically produce surface scattering due to their smoothness, which can sometimes resemble reflections from natural areas. By contrast, rough or uneven surfaces, even when bare, may produce volume scattering, further complicating the differentiation between man-made and natural structures in polarimetric SAR data.

This finding highlights a limitation of our approach, as current scattering decomposition and POA-based methods may not have the specificity required to distinguish between certain man-made and natural structures. These results suggest that incorporating additional polarization metrics or hybrid models with machine learning techniques could enhance the classification accuracy, particularly for identifying flat surfaces that might otherwise be misinterpreted as non-man-made areas.

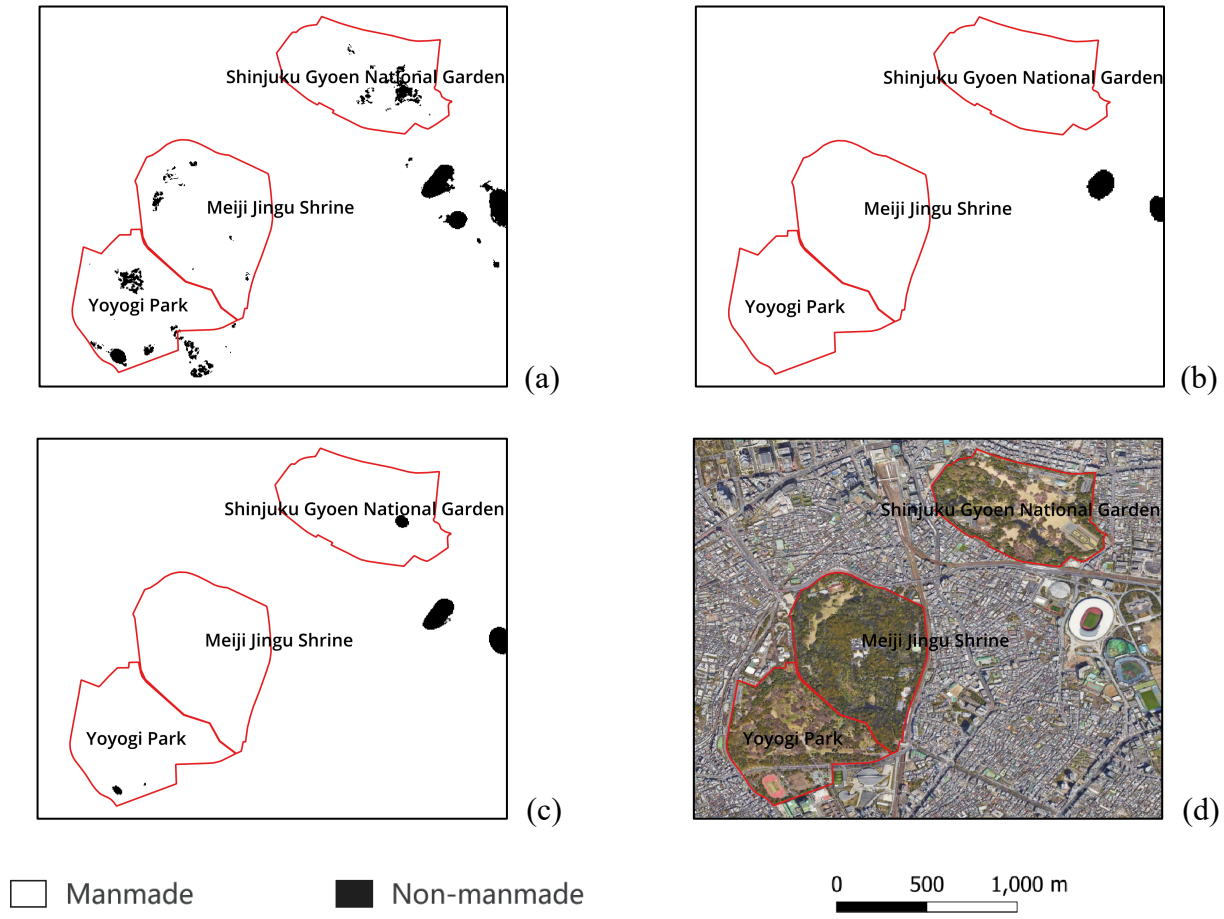

Figure 12: Close-up of the misclassification error, (a) misclassification error of the proposed method, (b) misclassification error using original scatterings, (c) misclassification error using scattering decompositions, and (d) optical reference from Google Earth.

5.8 Error Analysis and Future Improvements

Figure 12 illustrates examples of the misclassification errors in the different classification methods for the Tokyo area, specifically around Shinjuku Gyoen National Garden, Meiji Jingu Shrine, and Yoyogi Park. A

recurring issue is the confusion between volume scattering (Pv), typically associated with vegetation, and double-bounce scattering (Pd), which is characteristic of man-made structures. This misclassification is particularly noticeable in mixed-use zones and flat open surfaces.

Future research could explore incorporating additional polarization metrics or integrating machine learning techniques, such as deep learning, to further enhance the classification accuracy, particularly for differentiating man-made structures on flat surfaces. Although the POA-based method significantly improves classification, further refinement is necessary to address these specific misclassifications.

6. CONCLUSION AND RECOMMENDATION

This study explored various approaches for identifying man-made structures using Polarimetric Synthetic Aperture Radar (PolSAR) data and compared classification methods based on original scattering, scattering decomposition, and a combination of scattering decomposition and POA estimation. Although our method showed some improvements in accuracy, challenges remain in understanding the scattering behavior of man-made objects.

We validated our classification results against Advanced Land Observing Satellite-2/Phased Array-type L-band Synthetic Aperture Radar-2 (ALOS-2/PALSAR-2) data and the Sentinel-2 land-cover dataset, which focuses on dense human-made structures and provides a robust reference for evaluation. The manual exclusion of ground-level features, such as roads and parking lots, enabled a more precise assessment of our target structure.

The study findings include:

- **Misclassification of Vegetated Areas**: Confusion between volume and double-bounce scattering led to the occasional mislabeling of parks and forests as man-made structures.
- **Enhanced Detection of Elevated Structure**: While the original scatterings served as a baseline, scattering decomposition and POA estimation significantly improved the accuracy in identifying oriented structures such as buildings.
- **Focused Detection of Dense and Elevated Structure**: The method focused on dense, elevated structures, such as buildings and bridges, provides an effective approach for mapping man-made features. Roads and flat surfaces, which have lower-density signatures, are often not classified, enhancing the ability of the model to identify more significant infrastructure for urban planning.

Applying a mode or majority filter can help reduce noise and clarify the representations of man-made structures. This study confirms the value of advanced classification techniques in urban planning and infrastructure management, in which focusing on dense, elevated structures supports practical decision-making.

Future research can further enhance these results by incorporating a multi-frequency analysis and expanding the training datasets to include both dense and flat structures, creating a comprehensive classification approach. This approach enhances the accurate extraction of man-made structures from PolSAR data, providing vital support for effective man-made structure mapping, which is essential for

developing resilient and sustainable cities.

REFERENCES

Ainsworth, T. L., Schuler, D. L., and Lee, J.-S. 2008. "Polarimetric SAR Characterization of Man-Made Structures in Urban Areas Using Normalized Circular-Pol Correlation Coefficients." *Remote Sensing of Environment*, 112 (6): 2885–2976.

Breiman, L. 2001. "Random Forests." *Machine Learning*, 45 (1): 5–32.

Chaussard, E., Wdowinski, S., Cabral-Cano, E., and Amelung, F. 2014. "Land Subsidence in Central Mexico Detected by ALOS InSAR Time-Series." *Remote Sensing of Environment,* 140: 94–106.

Cloude, S.R., and Pottier, E. 1996. "A Review of Target Decomposition Theorems in Radar Polarimetry." *IEEE Transactions on Geoscience and Remote Sensing*, 34: 498-518.

Costa, J. D. S., Liesenberg, V., Schimalski, M. B., Sousa, R. V. d., Biffi, L. J., Gomes, A. R., Neto, S. L. R., Mitishita, E., & Bispo, P. d. C. (2021). Benefits of combining ALOS/PALSAR-2 and Sentinel-2A data in the classification of land cover classes in the Santa Catarina Southern Plateau. *Remote Sensing*, 13(2), 229.

Ferretti, A., Prati, C., and Rocca, F. 2000. "Non-Linear Subsidence Rate Estimation Using Permanent Scatterers in Differential SAR Interferometry." *IEEE Transactions on Geoscience and Remote Sensing*, 38: 2202–2212.

Ferretti, A., Fumagalli, A., Novali, F., Prati, C., Rocca, F., and Rucci, A. 2011. "A New Algorithm for Processing Interferometric Data-Stacks: SqueeSAR." *IEEE Transactions on Geoscience and Remote Sensing,* 49: 3460–3470.

Freeman, A., and Durden, S. L. 1998. "A Three-Component Scattering Model for Polarimetric SAR Data." *IEEE Transactions on Geoscience and Remote Sensing*, 36: 936–973.

Kajimoto, M., and Susaki, J. 2013a. "Urban-Area Extraction from Polarimetric SAR Images Using Polarization Orientation Angle." *IEEE Geoscience and Remote Sensing Letters,* 10: 337–341.

Kajimoto, M., and Susaki, J. 2013b. "Urban Density Estimation from Polarimetric SAR Images Based on a POA Correction Method." *IEEE Journal of Selected Topics in Applied Earth Observations and Remote Sensing*, 6: 1418–1429.

Karra, K., Kontgis, C., Statman-Weil, Z., Mazzariello, J. C., Mathis, M., and Brumby, S. P. 2021. "Global Land Use/Land Cover with Sentinel-2 and Deep Learning." In 2021 *IEEE International Geoscience and Remote Sensing Symposium (IGARSS),* 4704–4707. Brussels, 11–16 July 2021.

Kimura, H. 2008. "Radar Polarization Orientation Shifts in Built-Up Areas." *IEEE Geoscience and Remote Sensing Letters,* 5: 217–221.

Lee, Jong-Sen, D. L. Schuler, T. L. Ainsworth, E. Krogager, D. Kasilingam, and W.-M. Boerner. 2002. "On the Estimation of Radar Polarization Orientation Shifts Induced by Terrain Slopes." *IEEE Transactions on*

Geoscience and Remote Sensing, 40 (1): 30–41.

Lee, Jong-Sen, and Pottier, E. 2009. *Polarimetric Radar Imaging: From Basics to Applications*. 1st ed. Boca Raton: CRC Press.

Li, H., Q. Li, G. Wu, J. Chen, and S. Liang. 2016. "The Impacts of Building Orientation on Polarimetric Orientation Angle Estimation and Model-Based Decomposition for Multilook Polarimetric SAR Data in Urban Areas." *IEEE Transactions on Geoscience and Remote Sensing*, 54 (9): 5520–5532.

Niu, X., and Ban, Y. 2012. "An Adaptive Contextual SEM Algorithm for Urban Land Cover Mapping Using Multitemporal High-Resolution Polarimetric SAR Data." *IEEE Journal of Selected Topics in Applied Earth Observations and Remote Sensing*, 5: 1129–1139.

Shabou, A., Baselice, F., and Ferraioli, G. 2012. "Urban Digital Elevation Model Reconstruction Using Very High Resolution Multichannel InSAR Data." *IEEE Transactions on Geoscience and Remote Sensing*, 50: 4748–4758.

Srivally, M. V., Ghosh, S., Chaubey, N., Upadhyay, S., & Pandey, S. (2024). Analysis of different SAR polarimetric decomposition methods using EOS-04 polarimetric data for urban and natural features. In G. Dandabathula, A. K. Bera, S. S. Rao, & S. K. Srivastav (Eds.), *Proceedings of the 43rd INCA International Conference* (pp. 449–459). ISBN 978-93-341-2277-0.

Susaki, J., Kajimoto, M., and Kishimoto, M. 2014. "Urban Density Mapping of Global Megacities from Polarimetric SAR Images." *Remote Sensing of Environment,* 155: 334–348.

Wang, M., Liu, C., Han, D., Wang, F., Hou, X., Liang, S., & Sui, X. (2022). Assessment of GF3 full-polarimetric SAR data for dryland crop classification with different polarimetric decomposition methods. *Sensors*, 22(16), 6087.

Yamaguchi, Y., Yajima, Y., and Yamada, H. 2006. "A Four-Component Decomposition of POLSAR Images Based on the Coherency Matrix." *IEEE Geoscience and Remote Sensing Letters,* 3: 292–296.

Yamaguchi, Y. 2020. *Polarimetric SAR Imaging: Theory and Applications*. 1st ed. SAR Remote Sensing.